Passive 3D InISAR using target-borne illuminator of opportunity

Elisa Giusti
CNIT - RaSS National Laboratory
National Interuniversity Consortium for Telecommunication
Galleria G. Gerace, Pisa, Italy
Email: elisa.giusti@cnit.it

Marco Martorella
Department of Information Engineering
University of Pisa
Via Caruso 16, 56122, Pisa, Italy
Email: m.martorella@iet.unipi.it

***Abstract*—This paper proposes a new idea for forming 3D passive ISAR images. Two main innovations are presented, the first that is related to the use of a dual interferometer and the second that considers the illuminator of opportunity located on the target to be imaged. A theoretical approach was proposed in a previous paper that demonstrated passive ISAR imaging with a target-borne illuminator of opportunity in the 2D domain. In the present paper such approach is extended to a full 3D case. Simulations are used to produce some examples. Practical issues and limitations are also discussed in this paper.**

I. Introduction

Passive ISAR imaging has been proven possible provided that enough bandwidth and integration time are available for ISAR images to be formed with reasonable resolution [8]. Such ISAR images, although they do not produce similar results as dedicated active radar systems, are valuable for coarse classification purposes. Passive bistatic radar imaging at low frequencies may also provide the means for imaging low-observable targets.

Illuminators of opportunity that are typically chosen are broadcast radio and tv transmitters, which have a large EIRP and therefore provide larger coverage. [1], [4]–[6], [8], [12]. Nevertheless, several other types of illuminators of opportunity have been used in a number of passive radar applications, such as mobile phone communications [13] and wi-fi [3] among others. As such, IOs are typically installed on land and often only in populated areas,. This constraint makes passive radar viable only closely to IOs installation points, which limits passive radar applications, especially when it comes to open sea and deserted area surveillance. To overcome this issue, space-borne IOs have been considered, such as Satellite Digital TV Broadcast (DVB-S) [15], GPS/GNNS [7], [16], Space-borne SAR systems [11], etc., which offer continental scale coverage. Despite the great effort made in this direction, due to power limitation, the range coverage of passive radar based on space-borne illuminators still remains very limited.

A recent paper investigated the possibility of forming ISAR images when the illuminator of opportunity is on the target itself [9]. This could be the case of a target that uses communication systems, jammers or even its own radar. Being the transmitter in the same place as the target, the power budget becomes very favorable and, as far as such signals can be detected, an image of the target could be formed. Passive ISAR imaging with target-borne IOs may become then a complement to EW systems as they would provide extra information that may be used to identify the target based on its shape and size. In [9] the theoretical means to form ISAR images using target-borne IOs have been provided. However, the application of the proposed scheme was limited to the planar case (2D geometry). The transmitter proximity to the scatterers is the reason of the non linear relationship between the range/Doppler and the range/cross-range coordinates. This non-linearity affects the interpretation of a 2D ISAR image as it is no longer interpretable as a planar projection. In order to make such images interpretable, 3D reconstruction must be enabled. In this paper, 3D passive radar image formation is dealt with by introducing a dual interferometric system, which allows for orthogonal dual baseline interferometric phases to be exploited in conjunction with more traditional passive radar imaging for extracting target scatterers and positioning them in a 3D space. This paper is organised as follows. In Section II, the ISAR signal model is defined based on the radar-target geometry. The 2D range-Doppler passive radar image formation is shown in Section III whereas the 3D Passive ISAR image reconstruction technique is dealt with in Section IV. Section V defines the implementation steps that are necessary for implementing 3D reconstruction with a dual interferometric passive radar system and, finally, Section VI shows some simulation results.

II. ISAR signal model

Let be the geometry as represented in Figure 1. The receiver is composed of an L-shape antenna formed by three receiving elements (AV, AC, AH) located in a plane perpendicular to the Line of Sight (LoS) of the central element (AC), and d_V and dH are the two orthogonal baseline forming the L-shape.

Let $\mathbf{\Omega}_T$ and $\mathbf{\Omega}$ be the target rotation vector and the effective target rotation vector. $\mathbf{\Omega}$ is the component of $\mathbf{\Omega}_T$ which is responsible for the synthetic aperture formation and it lays in the plane perpendicular to the radar LoS. Let T_x be a reference system centered on the transmitter and embedded on the target such that x_3 and x_2 are aligned with $\mathbf{\Omega}$ and the LoS at the central time instant, respectively. Let T_y be another reference system which is rotated with respect to T_x of an angle ϕ which is the angle identifying the target effective rotation vector ($\mathbf{\Omega}$) orientation. According to this geometry, the receiver coordinates can be written in the T_x reference system as follows:

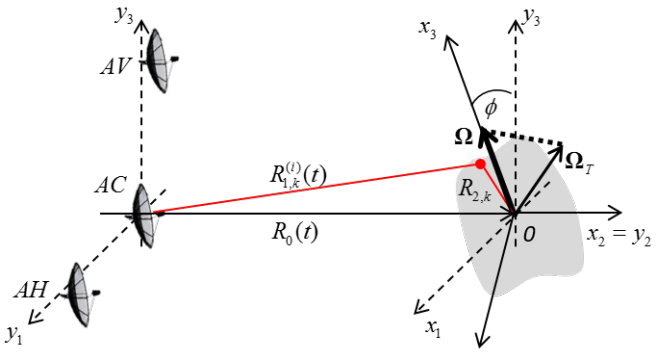

Fig. 1: System and target geometry

$$\begin{aligned} AV &= [d_V sin(\phi) \quad -R0 \quad d_V cos(\phi)]^T \\ AC &= [0 \quad -R0 \quad 0]^T \\ AH &= [-d_H cos(\phi) \quad -R0 \quad d_H sin(\phi)]^T \end{aligned} \tag{1}$$

where R_0 is the target-receiver distance at the time instant $t = 0$. Therefore, the LoS unit vectors can be derived as follows:

$$\begin{aligned} \mathbf{i}_{LoS}^{(AV)} &\simeq \left[-\frac{d_V}{R_0} sin(\phi) \quad 1 \quad \frac{d_V}{R_0} cos(\phi)\right]^T \\ \mathbf{i}_{LoS}^{(AC)} &\simeq [0 \quad 1 \quad 0]^T \\ \mathbf{i}_{LoS}^{(AH)} &\simeq \left[\frac{d_H}{R_0} cos(\phi) \quad 1 \quad -\frac{d_H}{R_0} sin(\phi)\right]^T \end{aligned} \tag{2}$$

$R_0(t)$, $R_{i,k}$ and $R_{T,k}$ are respectively, the distance between the target and the radar over time, the distance between the $i-th$ receiver (where $i \in [AC, AV, AH]$) and the $k-th$ scatterer over time, and the distance between the transmitter and the $k-th$ scatterer. As it can be noted $R_{T,k}$ does not depend on the time neither on the receiver.

We will consider a generic direct signal, which corresponds to the signal transmitted by the IO, as follows

$$s_0(t) = q_0 s_T(t - \tau_0(t)) \tag{3}$$

where $s_T(t)$ is the transmitted signal, q_0 is a complex amplitude and $\tau_0(t) = \frac{1}{c} R_0(t)$ is the delay-time variable relative to a point onto the target which in this case corresponds to the IO, as shown in Figure 1. The generic component reflected toward the $i-th$ receiver by a scatterer belonging to the target is as follows:

$$s_k^{(i)}(t) = q_k s_T(t - \tau_k^{(i)}(t)) \tag{4}$$

where q_k is the complex amplitude related with the $k-th$ scatterer, $\tau_k^{(i)}(t) = \frac{1}{c}\left(R_{i,k}(t) + R_{T,k}\right)$

The signal received by the $i-th$ receiver can be written as follows:

$$s_R^{(i)}(t) = s_0(t) + \sum_{k=1}^{K} s_k^{(i)}(t) \tag{5}$$

By assuming that we can separate the $s_0(t)$ component and by applying the Batches algorithm [14], the signal after the cross-correlation can be written as follows:

$$\begin{aligned} s_u^{(i)}(t,n) &= \int_{-\infty}^{\infty} s_R^{(i)}(\alpha, n) s_0^*(\alpha - t, n) d\alpha = \\ &= C_{s_0}(t,n) + s_b^{(i)}(t,n) \end{aligned} \tag{6}$$

where $n = [1, \cdots, N_b]$ is the batch index, N_b is the number of bathes such that $T_{obs} = N_b T_b$, T_{obs} and T_b are the observation time and the time length of a batch, $t \in [0, T_b]$ is the fast time variable, $C_{s_0}(t)$ is the auto-correlation function of the transmitted signal centered at $t = 0$, as defined in Equation (7)

$$\begin{aligned} C_{s_0}(t,n) &= q_0^2 \int_{-\infty}^{\infty} s_T(\alpha, n) s_T^*(\alpha - t, n) d\alpha = \\ &= q_0^2 C_T(t,n) \end{aligned} \tag{7}$$

and $s_b^{(i)}(t,n)$ is defined as in Equation (8)

$$s_b^{(i)}(t,n) = \sum_{k=1}^{K} q_0 q_k C_T(t - \Delta\tau_k^{(i)}(n), n) \tag{8}$$

By Fourier transforming $s_u^{(i)}(t,n)$ along t, the spectrum of $s_u(t,n)$, $P^{(i)}(f,n)$, can be written as follows:

$$\begin{aligned} &P^{(i)}(f,n) = \\ &= q_0^2 |S_T(f,n)|^2 + q_0 |S_T(f,n)|^2 \sum_{k=1}^{K} q_k e^{-j2\pi\Delta\tau_k^{(i)}(n)} \end{aligned} \tag{9}$$

where $S_T(f,n)$ is the Fourier transform of the transmitted signal within the $n-th$ batch, $\tau_k^{(i)}(t) \simeq \tau_k^{(i)}(n)$ (such an assumption is similar to the "stop & go "for SAR systems), and

$$\Delta\tau_k^{(i)}(n) = \frac{1}{c}\left[R_{i,k}(n) + R_{T,k} - R_0(n)\right] \tag{10}$$

In far-field condition (which now applies to the receivers) the "straight-iso-range"approximation holds, then $R_{i,k}(n)$ can be defined as:

$$R_{i,k}(n) \simeq R_0(n) + \mathbf{x}_k \cdot \mathbf{i}_{LoS}^{(i)}(n) \tag{11}$$

and therefore Equation (12) can be rewritten as follows:

$$\Delta\tau_k^{(i)}(n) = \frac{1}{c}\left[\mathbf{x}_k \cdot \mathbf{i}_{LoS}^{(i)}(n) + R_{T,k}\right] \tag{12}$$

By observing Equation (12), it can be noted that the radial motion compensation is not needed as it is embedded in the range-Doppler map formation.

III. 2D ISAR Image reconstruction

By assuming a constant target rotation vector during the Coherent Processing Interval (CPI), and following the results in [10] , Equation (9) can be approximated as follows:

$$P^{(i)}(f,n) = q_0^2 W(f,n) + q_0 W(f,n) \sum_{k=1}^{K} q_k e^{-j2\pi\frac{f}{c}\left(R_{T,k}+K_{0,k}^{(i)}\right)} e^{-j2\pi\frac{f_0}{c}K_{1,k}^{(i)}t} \tag{13}$$

where $W(f,n) = |S_T(f,n)|^2$ and

$$\mathbf{x}_k \cdot \mathbf{i}_{LoS}^{(i)} \simeq K_{0,k}^{(i)} + K_{1,k}^{(i)} \cdot t \tag{14}$$

A 2D ISAR image can be obtained at receiver can be obtained by applying a two-dimensional Fourier transform to Equation (13), thus obtaining:

$$I^{(i)}(\tau,\nu) \simeq q_0 \sum_{k=0}^{K} Q_k e^{-j2\pi\frac{f_0}{c}\tau_{k,i}} \text{sinc}\left(B(\tau-\tau_{k,i})\right) \text{sinc}\left(T_{obs}(\nu-\nu_{k,i})\right) \tag{15}$$

where $Q_k = q_k T_{obs} B$, $\tau_{k,i} = \frac{R_{T,k}+K_{0,k}^{(i)}}{c}$ and $\nu_{k,i} = K_{1,k}^{(i)}$. When $k=0$ (it corresponds to the transmitter location), both $\tau_{k,i}$ and $\nu_{k,i}$ equal 0.

When the baselines, d_V and d_H are small if compared to the target-receiver distance, $R_0(n)$, the range and Doppler coordinates in the argument of the sinc functions can be approximated as follows:

$$\tau_{k,i} \simeq \tau_{k,AC} = \tau_k = \frac{R_{T,k} + x_{k,2}}{c} \tag{16}$$

$$\nu_{k,i} \simeq \nu_k^{(AC)} = \nu_k = \frac{2f_0}{c}\Omega x_{k,1} \tag{17}$$

where $x_{k,1}$ and $x_{k,2}$ are the cross-range and range coordinates of the $k-th$ scatterer. This assumption does not apply for the phase term in Equation (18).

Therefore Equation (18) can be approximated as follows:

$$I^{(i)}(\tau,\nu) \simeq \sum_{k=0}^{K} q_k e^{-j2\pi\frac{f_0}{c}\left(R_{T,k}+K_{0,k}^{(i)}\right)} \text{sinc}\left(B(\tau-\tau_k)\right) \text{sinc}\left(\nu-\nu_k\right) \tag{18}$$

As it can be noted, the complex ISAR images are the composition of complex 2D sinc functions centered on the scatterer coordinates in the range/Doppler map. The phases of each sinc function depends on the path of the echo to go from the transmitter to the scatterer and then to a receiver. Then, it is worth to remark that when the 2D ISAR images are co-registered and the baselines are small if compared with the target-radar distance, the range/Doppler coordinates of the scatterers do not vary among the receivers. This is because the path differences are small if compared with the range/Doppler resolutions. This assumption does not apply to the phase term since the path differences are not negligible with respect to the wavelength $\lambda = \frac{c}{f_0}$.

IV. 3D target model reconstruction

The use of only the range and Doppler estimates extracted from the amplitude of the 2D ISAR images are not sufficient to recover the scatterer position in the T_x reference system. In fact, the range coordinate depends on $R_{T,k}$ (see Equation (16)) which corresponds to the scatterer Euclidean distance with respect to the center of the reference system, namely $R_{T,k} = \sqrt{\left(x_{k,1}^2 + x_{k,2}^2 + x_{k,3}^2\right)}$. To estimate the 3D scatterer coordinates, we need to use also the phase of the ISAR images, and specifically the interferometric phases, defined as follows:

$$\begin{aligned}\Delta\theta_V &= \angle\left(I^{AV}(\tau,\nu) \cdot \text{conj}\left(I^{AC}(\tau,\nu)\right)\right)\\ \Delta\theta_H &= \angle\left(I^{AH}(\tau,\nu) \cdot \text{conj}\left(I^{AC}(\tau,\nu)\right)\right)\end{aligned} \tag{19}$$

The phase terms in Equation (19) is a measure of the difference between the path the echo travels to go to the AV or AH receiver and the path the echo travels to go to the AC receiver. By using Equations (2) and (11), by noting that $R_{T,k}$ is the same for all the three receiver and by following the results in [10], the interferometric phases can be rewritten as follows:

$$\begin{aligned}\Delta\theta_{V,k} &= \frac{2\pi f_0 d_V}{cR_0}\left(x_{k,1}sin(\phi) + x_{k,3}cos(\phi)\right)\\ \Delta\theta_{H,k} &= \frac{2\pi f_0 d_H}{cR_0}\left(-x_{k,1}cos(\phi) + x_{k,3}sin(\phi)\right)\end{aligned} \tag{20}$$

The scatterers coss-range, x_1, and height, x_3, coordinates can be derived by manipulating Equation (20), as follows:

$$\begin{aligned}x_{k,1} &= \frac{cR_0}{2\pi f_0}\left(\frac{\Delta\theta_V}{d_V}sin(\phi) - \frac{\Delta\theta_H}{d_H}cos(\phi)\right)\\ x_{k,3} &= \frac{cR_0}{2\pi f_0}\left(\frac{\Delta\theta_V}{d_V}cos(\phi) + \frac{\Delta\theta_H}{d_H}sin(\phi)\right)\end{aligned} \tag{21}$$

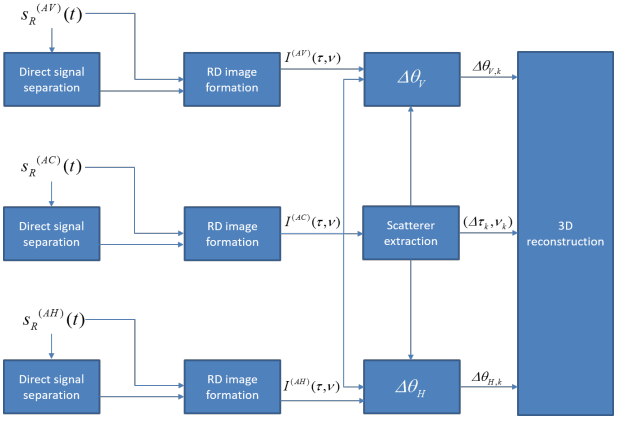

Fig. 2: functional block scheme of the proposed processing

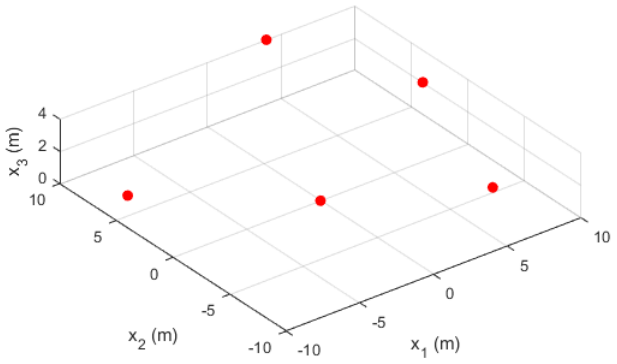

Fig. 3: Target point-like model

If we assume to a priori known both Ω and ϕ, the scatterer coordinates can be found by using $x_{k,3}$ as defined in Equation (21) and Equations (16), (17), as follows:

$$x_{k,1} = \frac{c\nu_k}{\Omega f_0} \tag{22}$$

$$x_{k,2} = \frac{\tau_k^2 - x_{k,1}^2 - x_{k,3}^2}{2 \cdot \tau_k} \tag{23}$$

The effective target rotation vector can be estimated by combining Equation (17) and $x_{k,1}$ in Equation (21), as follows:

$$\nu_k = \frac{\Omega R_0}{2\pi}\left(\frac{\Delta\theta_V}{d_V} sin(\phi) - \frac{\Delta\theta_H}{d_H} cos(\phi)\right) \tag{24}$$

Equation (24) can be rewritten as follows:

$$Z_k = aY_k + bX_k \tag{25}$$

where, $Z_k = \nu_k$, $Y_k = \frac{R_0 \Delta\theta_V}{2\pi d_V}$. $X_k = \frac{R_0 \Delta\theta_H}{2\pi d_H}$, $a = \Omega \cdot sin(\phi)$ and $b = \Omega \cdot cos(\phi)$. Equation (25) represents the equation of a 2D plane where Z_k, Y_k and X_k are all measured of the $k-th$ scatterer, and a and b have to be estimated. The unknown a and b can be estimated via a Least Square Error (LSE) approach and by minimizing the function in Equation (26). Further details can be found in [10].

$$\Psi_{(a,b)} = \sum_{k=1}^{K} [Z_k - (aY_k + bX_k)] \tag{26}$$

V. Target-borne IO passive 3D ISAR processing

Figure 2 shows the functional block scheme of the proposed processing.

The "direct signal separation step"aims at isolating the direct signal from the received one. In case of digital IOs, as for example frequency hopping phase coded modulated signals or OFDM signals, the direct signal separation can be performed by decoding the transmitted symbols and remodulating the signal, thus generating a synthetic version of the transmitted signal at the receiver. In case of moving platform, the channel temporal variation must be taken into account when decoding the transmitted symbols, as proposed in [2] for OFDM signals.

After forming 2D ISAR images through the "RD image formation"block, the dominant scatterers are extracted as well as their relative measures, τ_k, ν_k, $\Delta\theta_{V,k}$ and $\Delta\theta_{H,k}$. This set of values is then used to estimate Ω and ϕ by minimizing Equation (26), and to compute the scatterer coordinates, $(x_{k,1}, x_{k,2}, x_{k,3})$ by using Equations (23) and (21).

VI. Simulation results

In this section we present an example of the application of the proposed algorithm by using simulated data. The geometrical and radar parameters are as follows. The target is a simple point-like model, as shown in Fig. 3.

The target moves with respect to the radar with a constant velocity vector $v_t = [-40 \quad 40 \quad 56.57] m/s$ at a distance of about $6Km$ with respect to the radar. Additive White Gaussian Noise (AWGN) has been added to the target echo. The noise power is such that $SNR = 20dB$.

The modulus and phase of target effective rotation vector are, respectively, $\Omega = 0.0115 rad/s$ and $\phi = 2.1863$.

The range-Doppler maps at the output of the AC receiving channel is shown in Fig. 4. Similar ISAR images are obtained for the AV and AH channels.

It should be noted that the RD map does not represent the shape of the target as there is no linear relationship between the RD coordinates and the range/cross-range coordinates. The scatterer's position in the range-Doppler map are estimated by finding the range-Doppler map peaks. The scatterer's range and Doppler coordinates and interferometric phases are used to estimate the scatterer coordinates in the T_x reference system, according to Equations (23), (22) and (21).

The result is shown in Fig. 5 and Fig. 6, where the red dots represent the point-like target to be reconstructed, and the dark dots represents the reconstructed scatterer coordinates.

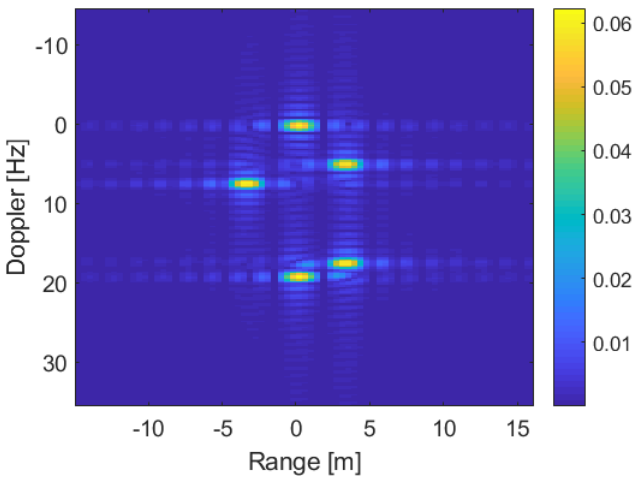

Fig. 4: 2D ISAR images relative to the AC channel

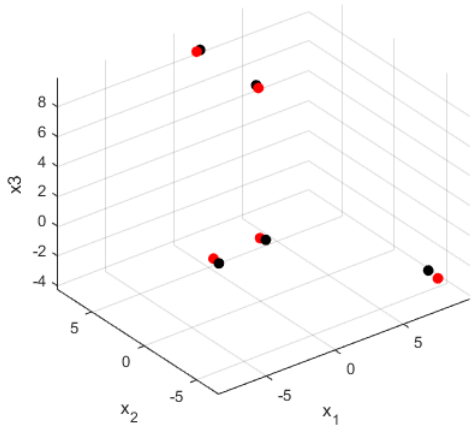

Fig. 5: 3D target model reconstruction

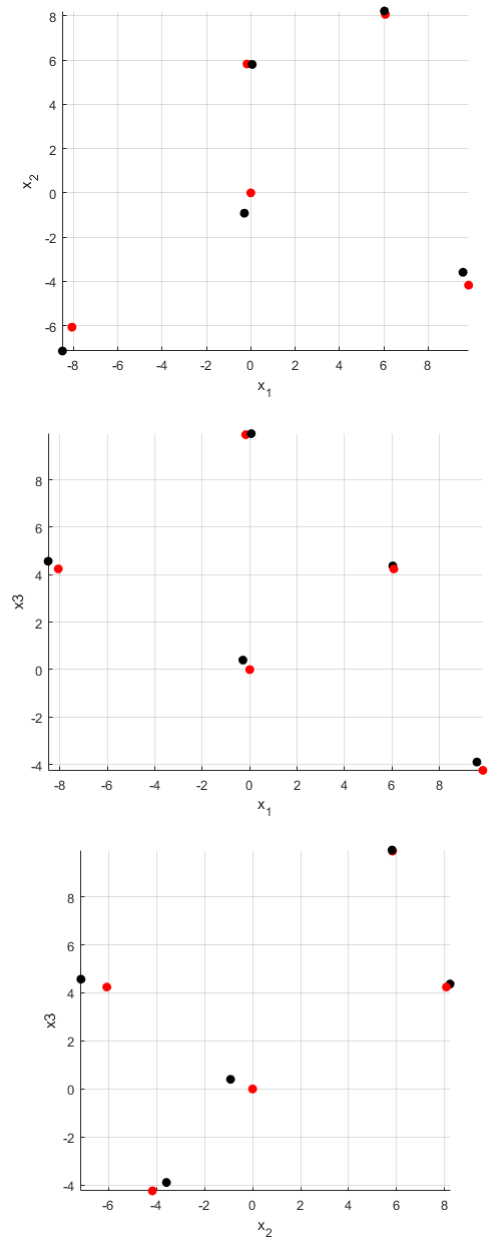

Fig. 6: 3D target model reconstruction as it appear in the 2D planes.

The estimated modulus and phase of the target effective rotation vector are, respectively, $\hat{\Omega} = 0.0127$ and $\hat{\phi} = 2.1314$ which are quite similar to the true ones. Therefore, both $x_{k,3}$ and $x_{k,1}$ are estimated with high accuracy. These estimates are then used to estimate $x_{k,2}$ through the Equation (23).

The estimation accuracy of $x_{k,2}$ depends both on the accuracy on the estimate of $x_{k,1}$ and $x_{k,3}$ and on the scatterer distance to the transmitters, namely the origin of the Cartesian reference system. In fact the more the scatterer is close to the Transmitter, the smaller the value of τ_k, which approaches zero, and the lower the accuracy in the estimation of the $x_{k,2}$ (due to the fact that τ_k appear at the denominator of Equation (23)).

VII. Conclusion

In this paper, a novel algorithm has been proposed to form 3D radar images by using a passive and interferometric radar system composed of three receiving antennas and by exploiting target-borne IOs. The theoretical aspects have been laid in this paper and some preliminary simulation results have have been shown as examples. This is fundamentally a research work in progress. Some additional efforts are necessary for dealing with the direct signal separation. Also the effects induced by transmitted waveform have not been analysed in details. This will also be part of future research activities. Some refinements and additional results may be added to the final paper.

References

[1] C.J. Baker, H.D. Griffiths, and I Papoutsis. Passive coherent location radar systems. part 2: waveform properties. *Radar, Sonar and Navigation, IEE Proceedings* -, 152(3):160–168, June 2005.

[2] C. Berthillot, A. Santori, O. Rabaste, D. Poullin, and M. Lesturgie. Improving bem channel estimation for airborne passive radar reference signal reconstruction. In *2015 16th International Radar Symposium (IRS)*, pages 77–82, June 2015.

[3] P. Falcone, F. Colone, A. Macera, and P. Lombardo. Two-dimensional location of moving targets within local areas using wifi-based multistatic passive radar. *IET Radar, Sonar Navigation*, 8(2):123–131, February 2014.

[4] A. Farina and H. Kuschel. *Aerospace and Electronic Systems Magazine, IEEE*, 27(10):5, 2012.

[5] H.D. Griffiths and C.J. Baker. Passive coherent location radar systems. part 1: performance prediction. *Radar, Sonar and Navigation, IEE Proceedings -*, 152(3):153–159, June 2005.

[6] P. Howland. Editorial: Passive radar systems. *Radar, Sonar and Navigation, IEE Proceedings -*, 152(3):105 – 106, june 2005.

[7] F. Liu, M. Antoniou, Z. Zeng, and M. Cherniakov. Coherent change detection using passive gnss-based bsar: Experimental proof of concept. *IEEE Transactions on Geoscience and Remote Sensing*, 51(8):4544–4555, Aug 2013.

[8] M. Martorella and E. Giusti. Theoretical foundation of passive bistatic isar imaging. *IEEE Transactions on Aerospace and Electronic Systems*, 50(3):1647–1659, July 2014.

[9] M. Martorella, E. Giusti, and W.Nel. Passive isar using target-borne illuminators of opportunity. In *International Conference on Radar Systems - Radar 2017*, 2017.

[10] M. Martorella, D. Stagliano, F. Salvetti, and N. Battisti. 3d interferometric isar imaging of noncooperative targets. *IEEE Transactions on Aerospace and Electronic Systems*, 50(4):3102–3114, October 2014.

[11] L. Maslikowski, P. Samczynski, and M. K. Baczyk. X-band receiver for passive imaging based on terrasar-x illuminator. In *Signal Processing Symposium (SPS), 2013*, pages 1–4, June 2013.

[12] W. L. Melvin and J. A. Scheer. *Principles of modern radar: advances techniques*. Scitech publishing, 2012.

[13] D. Petri, F. Berizzi, M. Martorella, E. D. Mese, and A. Capria. A software defined umts passive radar demonstrator. In *11-th INTERNATIONAL RADAR SYMPOSIUM*, pages 1–4, June 2010.

[14] D. Petri, C. Moscardini, M. Martorella, M. Conti, A Capria, and F. Berizzi. Performance analysis of the batches algorithm for range-doppler map formation in passive bistatic radar. In *Radar Systems (Radar 2012), IET International Conference on*, pages 1–4, Oct 2012.

[15] S. Ribo, J. C. Arco, S. Oliveras, E. Cardellach, A. Rius, and C. Buck. Experimental results of an x-band paris receiver using digital satellite tv opportunity signals scattered on the sea surface. *IEEE Transactions on Geoscience and Remote Sensing*, 52(9):5704–5711, Sept 2014.

[16] F. Santi, M. Antoniou, and D. Pastina. Point spread function analysis for gnss-based multistatic sar. *IEEE Geoscience and Remote Sensing Letters*, 12(2):304–308, Feb 2015.